ChemElectroChem

Chemistry Europe
European Chemical Societies Publishing

Accepted Article

Title: Developing N-Rich Carbon from C3N4-Polydopamine Composites for Efficient Oxygen Reduction Reaction

Authors: Zhaolin Liu, Beatriz Ferraz, Bing Li, Zhengxiao Guo, and Christopher Blackman

To be cited as: *ChemElectroChem* 10.1002/celc.202100865

Link to VoR: https://doi.org/10.1002/celc.202100865

WILEY-VCH

10.1002/celc.202100865

WILEY-VCH

ARTICLE

Developing N-Rich Carbon from C_3N_4-Polydopamine Composites for Efficient Oxygen Reduction Reaction

Beatriz J. Ferraz [a] [b], Bing Li [b], Zhengxiao Guo [a] [c] [d], Christopher Blackman [a] and Zhaolin Liu* [b]

[a] Ms. B. J. Ferraz, Prof. Z. X. Guo, Prof. C. Blackman
Department of Chemistry
University College London
20 Gordon Street
London, WC1H 0AJ, UK

[b] Ms. B. J. Ferraz, Dr. Z. Liu, Dr. B. Li
Institute of Materials Research and Engineering, Agency for Science, Technology and Research (A*STAR),
2 Fusionopolis Way, Innovis, #08-03,
Singapore, 138634, Singapore
E-mail: zl-liu@imre.a-star.edu.sg

[c] Prof. Z. X. Guo
Zhejiang Institute of Research and Innovation, The University of Hong Kong ,
Qingshan Lake Scitech City, Hangzhou, PR China

[d] Prof. Z. X. Guo
Department of Chemistry and Mechanical Engineering,
The University of Hong Kong,
Hong Kong SAR, PR China

Supporting information for this article is given via a link at the end of the document.

Abstract: In Nitrogen-rich carbon-based materials are amongst the most promising electrocatalysts for the oxygen reduction reaction (ORR) and/or the oxygen evolution reaction (OER). The introduction of nitrogen within the carbonaceous framework generates catalytic active sites and alters the electrical conductivity. However, the synthesis of these materials often involves long processes and severe reaction conditions which yield a low concentration of nitrogen (N) functionalities. Herein, we present a facile method for the synthesis of N-rich carbon by carbonizing a carbon nitride (C_3N_4)-polydopamine composite (CNDA) which can readily be prepared by room temperature self-polymerisation of dopamine in the presence of C_3N_4. The intrinsically high N content in C_3N_4 leads to a highly N-doped carbon. The CNDA catalyst synthesized at 900 ºC contained 12.5 at% of N, enhancing both the ORR and OER catalytic activities through a 4-e^- dominated pathway, providing a comparable $E_{1/2}$ and a remarkably improved diffusion-limited current to the other reported N-doped carbon catalysts. When used as an air-cathode in a zinc-air battery, this CNDA catalyst possessed stable discharge-charge cycling performance for 216 h, outperforming the Pt/C standard. This work opens a promising platform for the development of template-free processes for the synthesis of non-metal and nitrogen-rich carbon materials which are attractive for metal-air batteries and fuel cells.

Introduction

Increasing consumption of energy worldwide, and growing interest in smart grids and electrification of vehicles, has driven interest in electrochemical energy storage and conversion technologies. Zinc-air batteries (ZABs) are particularly attractive compared to commonly used lithium-ion batteries due to their considerably higher theoretical energy density (1086 Wh kg^{-1}), lower cost and better safety attributes.[1,2] In ZABs the oxygen reduction reaction (ORR) is an essential process driving the discharging reaction at the cathode.[3] However, the high O=O bond energy (~498 kJ mol^{-1}) requires electrocatalysts to facilitate this reaction by improving its kinetics.[4,5] The oxygen evolution reaction (OER) is the reverse reaction that takes place during the charging process.

Currently, precious metal-based electrocatalysts, such as platinum (Pt) and iridium (Ir), are still widely used and set the benchmark performance for ORR and OER, respectively. However, their scarcity, high cost and fast degradation, together with unsatisfactory long term stability, limit the development and commercialization of ZABs.[6] Consequently, great efforts have been focused on the development of alternative electrocatalysts with comparable performance to those of precious metals.[7–10] Promising advances have been observed in such developments, especially those carbonaceous materials enriched with heteroatoms such as N, S, P and B.[4,5,11–18] Their low cost and environmentally friendly nature together with properties of high surface area, facile tailoring and good electronic conductivity make carbonaceous materials ideal choices for ORR electrocatalyst developments. Additionally, the incorporation of nitrogen (N) within carbon nanostructures could induce a charge delocalization on the carbon atoms, disturbing the electroneutrality, leading to narrowing of the band gap and enhanced electron mobility promoting the adsorption and reduction of oxygen.[19,20]

The majority of the reported N-doped carbon catalysts are synthesised by post-doping methods which require the introduction of nitrogen functionalities into the highly stable carbon framework. These typically involve hydrothermal synthesis, acid exfoliation or surface functionalization with gas. Such methods often include the use of autoclaves, harsh

chemicals and long and unsafe processes which only yield surface doping, limiting the scalable production of such materials.[12,21–24] *In situ* direct doping methods involve less intensive synthesis processes, however the nitrogen concentration achieved is typically low (below 9 at.%) or unexposed, limiting the number of redox active centres.[23,25] Additionally, to control the surface morphology and increase the surface area, templates such as silica, cellulose and polystyrene are commonly employed and finally removed by immersion in organic solvents or by toxic solvents such as HF.[18,26,27] Thus, the development of a facile method for the synthesis of efficient metal-free electrocatalysts with a high level of nitrogen doping whilst avoiding the use of toxic chemicals and severe conditions is highly desirable.

Herein, a facile and template-free process for the synthesis of carbon materials with high nitrogen content (12.5 at.%) is demonstrated. The incorporation of two benign and scalable precursors, yielded a carbon nitride (C_3N_4) and dopamine (DA)-derived electrocatalyst (CNDA), composed of non-metal nitrogen-rich carbon nanosheets and nanospheres. The CNDA catalyst demonstrated enhanced and durable activity towards the ORR due to exposed and stable active sites. C_3N_4 was employed due to its naturally rich nitrogen content (47.75 %) which facilitates the interactions with the ORR intermediates. C_3N_4 also served as a porogen and a surface template for the growth of dopamine (DA). Unlike other N-doped carbons,[28,29] C_3N_4 is synthesised by an easily scalable, high yield and safe process which does not require post doping or the removal of metal impurities. However, it's poor electrical conductivity and, therefore, slow charge transfer hinders its electrocatalytic ability.[30] Consequently, polydopamine (PDA), an N-containing biopolymer found in mussels which allows their firm adhesion to surfaces, was incorporated due to its tendency for surface functionalization and electrophilicity. Dopamine easily self-polymerizes to form PDA at room temperature in a mild and alkaline environment.[31] This synthesis is performed without the use of catalysts or severe conditions commonly used for polymers of aniline, pyrrole and o-phenylenediamine.[32] During pyrolysis, the PDA coating yielded the formation of high-quality carbon layers with enhanced electron mobility capability due to improved electrical conductivity and stability of the active materials. This is an indispensable feature for the good performance of oxygen electrocatalysts.[33] The addition of PDA was essential to prepare the carbon materials, evidenced by the fact that pure C_3N_4 completely decomposed under the same pyrolysis conditions without any PDA addition. We concluded that the introduction of PDA allowed the doping of extra nitrogen features from species originated from the decomposition of C_3N_4.[34] The high temperature pyrolysis (900 °C) afforded the fusion of the two carbon-based precursors resulting in an efficient nitrogen-doped nanocarbon ORR electrocatalyst.

Results and Discussion

The synthesis procedure of the N-rich carbon catalyst, CNDA, is depicted in Scheme 1. First, C_3N_4 was obtained by thermal polymerization of melamine. Subsequently, a C_3N_4-PDA composite was formed by a spontaneous oxidation polymerization reaction of DA in the presence of C_3N_4 layers. During polymerization, PDA can adhere to the surface of C_3N_4. Finally, carbonizing the composite at a temperature between 900 °C under Ar protection lead to the fusion of the structures due to a chemical rearrangement of the carbon and heteroatoms, producing a N-rich carbon (CNDA900). The introduction of PDA allowed the stabilization of C_3N_4, avoiding its decomposition and therefore benefiting from its rich N content.

The structures and morphologies of the bulk C_3N_4, carbonized-PDA (CPDA) and the CNDA catalysts were observed using SEM and TEM and the elemental mappings obtained by EDX revealed their elemental distributions. The bulk C_3N_4 (Figure 1a) presented the typical aggregate morphology of C_3N_4, but also containing some stacked nanosheet structures indicating some level of exfoliation due to the high temperature carbonization. In Figure 1b, the structure of the CPDA shows the uniform distribution of spherical structures with sizes of about 200 nm. The SEM

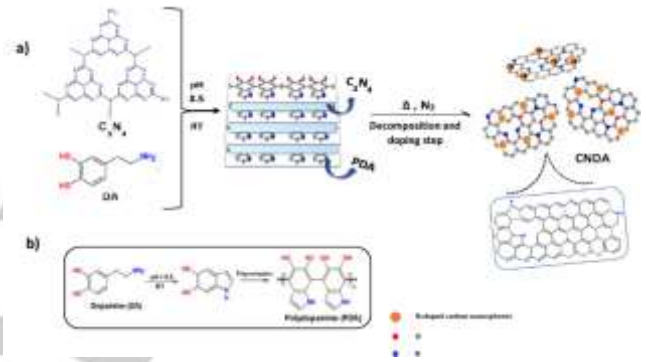

Scheme 1. A) Schematic representation of the fabrication of the CNDA catalysts and b) the polymerization of dopamine (DA) to form polydopamine (PDA).

image of CNDA900 catalyst indicates the formation of uniformly distributed nanospheres across structured layers (Figure 1d). However, heating at 950 °C created over-exfoliated nanosheets with large clusters (Figure S1) which may relate to folded carbon layers that then reduce the active sites' availability and limit the reduction of oxygen.[35,36] The incomplete carbonization observed on the Scanning Electron Microscope (SEM) and (Transmission Electron Microscope) (TEM) images of the CNDA850 catalyst is confirmed by the uneven distribution of nanoparticles with various sizes (~ 150-250 nm) on the surface of a dense structure (Figures S2). This further confirmed the crucial role of pyrolysis temperature on the surface structure formation which controls the catalytic activity of the catalysts. The TEM image of CNDA900 (Figure 1c) further confirmed the presence of well-shaped and size controlled (~190 nm) nanospheres interconnected with thinner and well-defined nanolayers. The decreased number of nanospheres and improved nanosheet scattering indicated the successful conversion of the reaction intermediates into an N-doped carbon framework and the effective role of C_3N_4 as a surface growth template. This configuration is expected to enable a more efficient catalytic surface favouring a faster electron and mass transport.[37] The elemental distribution maps of CNDA900 (Figure S3) confirm the uniform distribution of C, N and O. This is expected to allow the activation of catalytic sites across the catalyst's surface due to the synergistic effect induced by the doping of elements with distinct electronegativities.[17,38] Besides

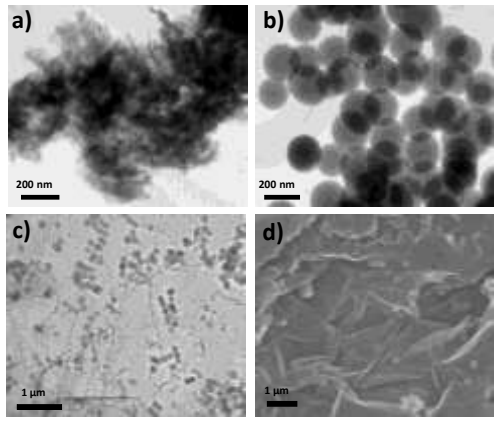

Figure 1: TEM images showing the morphologies of a) C_3N_4, b) CPDA and c) CNDA900. d) SEM image of CNDA900.

controlling the surface growth of polymerized DA, C_3N_4 also clearly contributed as the nitrogen source for the synthesis of CNDA900.

The elemental and chemical environment stoichiometry of C_3N_4, CPDA and the CNDA catalysts were investigated by X-ray Photoelectron Spectroscopy (XPS) analysis. The XPS survey spectra presented in Figure S4 and Table S1 further confirm that both precursor materials, CPDA and C_3N_4, and the CNDA catalysts' surfaces are composed of C, N and O. As the annealing temperature was increased, the nitrogen content reduced. CNDA900 was found to contain 12.5 at.% of nitrogen in its surface composition, which is higher than many reported nitrogen-doped carbon electrocatalysts.[39–41] This indicates the adherence of CPDA to C_3N_4 as CPDA was only found to contain 5.3 at.% of N. An increased annealing temperature to 950 °C greatly reduced the N content to 6.3 at.%. The C1s XPS spectra of CPDA, C_3N_4 and CNDA900 are depicted in Figure 2a. The C1s XPS spectrum of CPDA was deconvoluted into four peaks at 284.4 (sp^2 C), 285.6 (C-O and C=N), 287.1 (C-O-C) and 288.7 eV (C-N).[42,43] Two peaks at 284.3 and 287.8 eV were fitted on the XPS C1s spectrum of C_3N_4, indicating the presence of sp^2 C and N-C-$(N)_2$ features.[44] The XPS spectrum for C1s of CNDA900 presents a very similar pattern to that of CPDA suggesting that CNDA900 is principally CPDA in character, yielding the conductive carbon layers. Figure 2b exhibits the N1s XPS spectra of CPDA, C_3N_4 and CNDA900. The two fitted N1s XPS peaks for CPDA centred at 399.7 and 402.3 eV refer to the pyrrolic and graphitic N, respectively.[43] Four peaks were fitted on the XPS N1s spectrum of C_3N_4 presented above, 398.3, 399.4, 400.7 and 404.1 eV, corresponding to the sp^2-bonded aromatic N (C-N=C), tertiary N [N-$(C)_3$], terminal amino groups (C-N-H) and positive charge localization due to imperfect polymerization, respectively.[44–46] The XPS N1s spectrum for CNDA900 can be deconvoluted into four different bands at 398.1 (46.3 at. %), 399.3 (15.4 at. %), 400.8 (31.8 at. %) and 402.6 eV (6.4 at. %), which present a pattern close to that observed for C_3N_4, indicating the origin of the principal N species of CNDA900. However, the overlap of the pyrrolic N binding energy from CPDA with the energy of the N-$(C)_3$ bonds from C_3N_4 contribute to the increased intensity of the fitted peak at 399.3 eV of CNDA900. The peak at 402.6 eV confirms the presence of some graphitic-N environments on the structure of CNDA900. The N 1s spectra of CPDA is composed of two similar peaks with

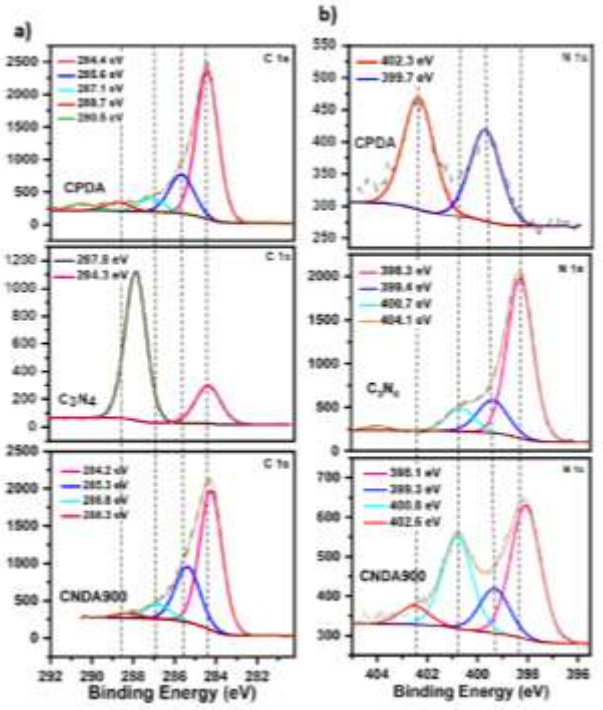

Figure 2: High-resolution XPS spectra of CPDA, C_3N_4 and CNDA900: a) C 1s and b) N 1s.

an area ratio of approximately 1:1, but the equivalent peaks in CNDA900 are observed with a ratio of about 3:1 (lower energy : higher energy) arising from the contribution of both PDA and C_3N_4 to the intensity of the lower energy peak. These results further indicate that PDA helps supressing the volatilization of C_3N_4 and subsequent loss of N species leading to an increased active sites concentration.

The Raman spectra of CNDA850, CNDA900, CNDA950 and CPDA (Figure S5) revealed their degree of defective and graphitic character from the observation of the typical D and G bands at approximately 1350 and 1580 cm^{-1}, respectively.[15] The I_D/I_G band intensity ratios of CNDA900 and CNDA9 50 were 0.999 and 0.996, respectively, indicating a slightly higher level of graphitization with increasing carbonization temperature. The generation of defects indicated by the D band can be attributed to the successful doping of nitrogen atoms and surface distortion.[15,43] In the case of CNDA850, both intensities for I_D and I_G were very low, implying a low content of graphite related structures formed at 850 °C. The addition of C_3N_4 to CPDA and further carbonization, improved the graphitic character and reduced the number of defects on the final product, which is confirmed by a lower I_D/I_G ratio in comparison to CPDA (I_D/I_G= 1.024). This graphitic character could facilitate the electron and mass transfers to the active sites and therefore promoting the ORR.[47]

The X-ray diffraction (XRD) patterns of CPDA in Figure S6 showed a broad diffraction peak at 22.3°, suggesting its amorphous nature.[48] The characteristic sharp XRD peak detected at 27.6° for C_3N_4 is owing to the interlayer stacking of C_3N_4, in agreement with previous reports.[44] CNDA900 presented a least broad peak and slightly positively shifted peak at around 23.8°, suggesting some extent of improvement of graphitic-like

phases as compared to the CPDA, despite an overall amorphous nature of CNDA900. This was also previously suggested by the increased graphitic (G) band intensity observed in the Raman spectra of CNDA900 (Figure S5) in comparison to that of CPDA. The XPS, Raman and XRD results confirmed the essential contribution of each of the reaction precursors on the formation of the catalysts' structure.

The electrocatalytic performance of the CNDA hybrid catalysts, CPDA and C_3N_4 were comparatively studied in 0.1 M KOH electrolyte. The cyclic voltammetry (CV) curves of all the CNDA catalysts (Figure 3a and Figure S7a) exhibited oxygen reduction peaks in the O_2-saturated solution but no distinct features were observed in the N_2-saturated solution, confirming the ORR catalytic activities of the prepared catalysts. The reduction potential peak of CNDA900 at 0.812 V versus reversible hydrogen electrode (RHE) was comparable to the peak of the commercial Pt/C (20 wt.%) catalyst (0.822 V), and more positively shifted as compared to the CNDA950 sample (0.762 V, Figure S7a). The bare CPDA and C_3N_4 precursors were less active to reduce oxygen making them unsuitable catalysts for the ORR (Figure S7b). Linear sweep voltammetry curves (LSV) and kinetic

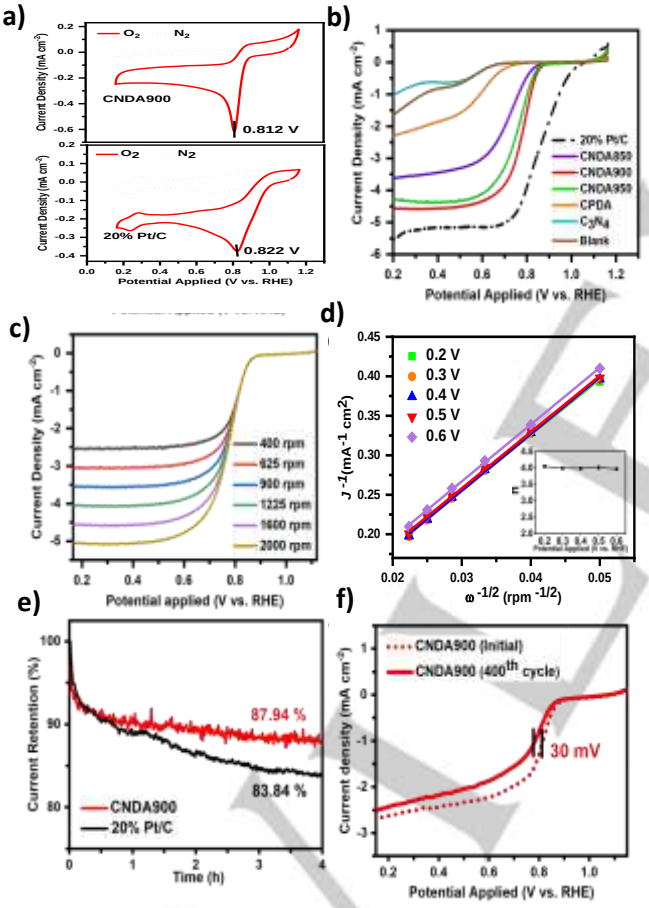

Figure 3: a) CV curves of the CNDA900 catalyst and Pt/C obtained in N_2/O_2-saturated 0.1 M KOH electrolyte. b) Combined LSV curves for ORR of all the CNDA catalysts, CPDA, C_3N_4 and Pt/C at 1600 rpm. c) LSV curves of CNDA900 recorded at different rotation speeds (rpm). d) K-L plots of CNDA900 calculated from its RDE LSV curves at the potential range 0.2-0.6 V vs. RHE; the inset: plot of n (electron transfer number) per O_2 molecule at the different potentials. e) Chronoamperometric stability plots (i-t plots) of CNDA900 and Pt/C at 0.4 V and a fixed electrode rotation speed of 400 rpm. f) ADT plots of CNDA900 before (dashed lines) and after (solid lines) 400 cycles for ORR at a fixed electrode rotation speed of 400 rpm. The scan rate was kept at 5 mV s^{-1} for all the measurements.

current vs. potential relations were also collected for the catalysts and are compared in the Figure 3b and Figure S8. Clearly, all three CNDA catalysts showed improved catalytic activity towards ORR, confirming the successful interactions between PDA and C_3N_4.The combination of these two π-conjugated polymers lead to a more efficient electron mobility and active sites formation. The introduction of extra N species in the carbon architecture can introduce a charge delocalisation on the adjacent C creating these catalytically active sites.[16,49] Particularly, the CNDA900 was found to provide the best performance with a more positively shifted LSV curve and the highest diffusion-limited current density among CNDA, CPDA and C_3N_4 catalysts. The diffusion-limited current density for CNDA900 was 4.60 mA cm^{-2}, surpassing CNDA850 (3.67 mA cm^{-2}) and CNDA950 (4.26 mA cm^{-2}) and just 0.90 mA cm^{-2} lower than that of the commercial Pt/C catalyst (5.50 mA cm^{-2}). The half-wave potential ($E_{1/2}$) of CNDA900 at 0.78 V was only 0.08 V more negative than that of the Pt/C benchmark (0.86 V), but 0.05 and 0.02 V positively shifted as compared to the CNDA850 and CNDA950, respectively. The CNDA900 demonstrated a comparable $E_{1/2}$ to that of other reported N-doped carbon catalysts and a remarkably improved diffusion-limited current density.[14,15] In comparison with some reported metal-based ORR electrocatalysts, ours achieved an enhanced current density, despite being metal-free.[50,51] These results confirmed that CNDA900 has a superior ORR catalytic activity on par with other high-performance ORR catalysts reported in literature (Table S2). The inferior performance of the CNDA850 and CNDA950 catalysts may be due to the reduced exposure, heterogeneous distribution of the active sites or decomposition of dopants due to overheating leading to a higher charge-transfer resistance.

To determine the electron transfer number per oxygen molecule (n) and therefore better understand the ORR activities of the catalysts, Koutecky-Levich (K-L) relations were deduced from the measured current densities at different rotations (Figure 3c). The wide and steady plateau observed from the LSV of CNDA900 suggest a diffusion-controlled ORR.[16] The steady, linear and parallel slopes of the CNDA900 K-L plots (Figure 3d) indicate first-order reaction kinetics with respect to the concentration of oxygen dissolved in the electrolyte.[31,52] The average n value of CNDA900 was calculated to be approximately 4.00 for the potential range of 0.2-0.6 V vs. RHE, confirming a favourable 4-electron pathway, which is comparable to the benchmark ORR catalyst of Pt/C.[15] The average n values deduced from the K-L plots for CNDA850 and CNDA950 (Figure S9) were 3.65 and 4.23, respectively, indicating a sluggish oxygen reduction reaction and possible side reactions taking place.

Long-term catalytic stability is of great importance for practical zinc-air battery applications. To accelerate the accessing process of the catalyst catalytic stability, we conducted chronoamperometric (*i-t*) measurements at a fixed potential of 0.40 V (vs. RHE) under the RDE rotating at 400 rpm. At 0.40 V (vs. RHE) the RDE reached its ORR limiting current density will inevitably stress the catalyst and make it more vulnerable to chemical and mechanical damages. While the RDE rotating at 400 rpm can resulting in the electrolyte solution continuously "flush" the catalyst at the electrode surface, in turn, increases the likelihood of catalyst detachment and hence accelerate the catalytic performance degradation. Therefore, the *i-t* test at such stringent conditions provides accelerated degradation data of the catalyst and facilitates the development of robust catalysts for

more durable zinc-air batteries. Figure 3e shows the i-*t* test data, after a 4 h continuous test the current retention of its initial ORR current for CNDA900 was about 87.94 %, clearly higher than that of the benchmark ORR catalyst of Pt/C (83.84 %) under the same testing conditions. These results unambiguously demonstrated the good ORR durability of CNDA900 as compared to the commercial Pt/C, although efforts including post-characterizations are recommended to precisely understanding the reason for the stability decay for future studies. The ORR durability of CNDA900 was further evidenced by accelerated degradation test (ADT) results (Figure 3f) in which the LSV curve of CNDA900 only shifted 30 mV at the current density of 1 mA cm^{-2}. These results suggest the presence of multiple electron transfer channels on CNDA900 allowing the continuous catalytic reactions to take place.

Apart from being highly efficient at promoting ORR with good stability, the CNDA900 was also found capable of catalysing OER. The LSV curve of CNDA900 (Figure S10) shows an increase in anodic current above 1.23 V, achieving a lower onset potential than that of Pt/C at 1.57 V and a higher current density. The CNDA900 catalyst also presents an enhanced OER performance as compared to the CNDA850 and CNDA950, though inferior to that of the benchmark OER catalyst, Ir/C.

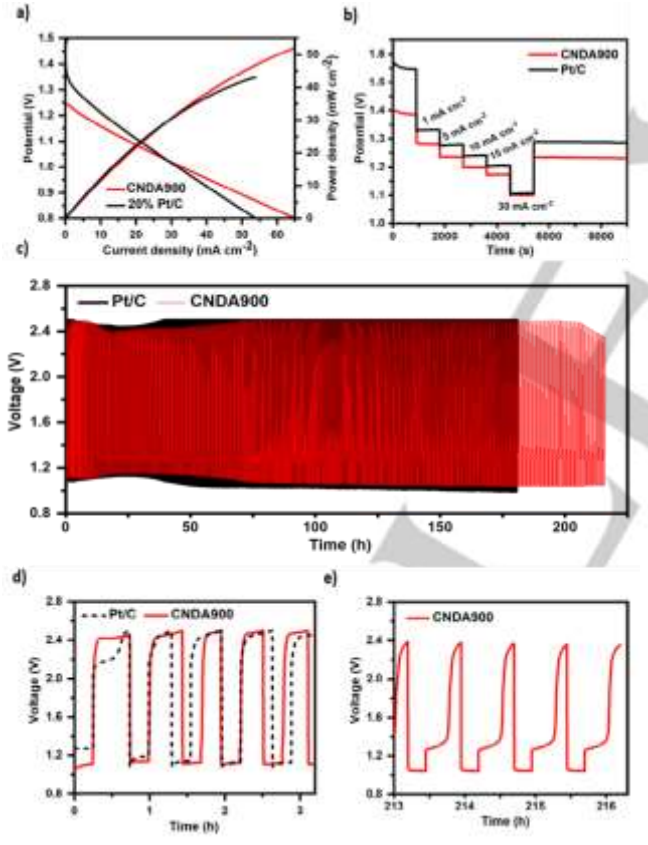

Figure 4: a) Polarization and power density curves of ZABs using CNDA900 and Pt/C as ORR catalyst with a mass loading of 0.5 mg cm^{-2} in 6 M KOH electrolyte and a scan rate of 5 mV s^{-1}. b) Voltage profiles of CNDA900 and Pt/C based ZABs when discharged at different current densities: 1, 5, 10, 15 and 30 mA cm^{-2}. c) Discharge-charge cycling performances of ZABs with CNDA900 and Pt/C catalysts. d and e) Selected sections of the cycling performances from c).

The above electrochemical studies suggested CNDA900 was an efficient and durable ORR catalyst and capable of promoting OER, which could be suitable for Zn-air battery applications. Prototype ZABs were assembled using CNDA900 electrocatalyst in the air cathode and compared to an air cathode assembled with Pt/C. The polarization and power density curves are presented in Figure 4a, the cell with CNDA900 catalyst showed an increase of current density with decreasing voltage. At 0.8 V, the CNDA900 catalyst achieves a current density of 65 mA cm^{-2} and a power density of 52 mW cm^{-2}, respectively, both of which are higher than that delivered by the Pt/C catalyst, being 54 mA cm^{-2} and 43 mW cm^{-2} for current density and power density, respectively. The comparison of the power density of assembled zinc-air batteries with previous publications are shown in Table S3.

Figure 4b presents the galvanostatic discharge results of CNDA900 and Pt/C catalysts in ZABs at different current densities: 1, 5, 10, 15 and 30 mA cm^{-2}. The cell with CNDA900 catalyst demonstrated a good rate performance with stable and flat discharge voltage plateaus observed at various current densities. Particularly, the battery achieved a high discharge voltage of 1.1 V even at a discharge current density as high as 30 mA cm^{-2}, which is merely 10 mV lower than the cell with Pt/C catalyst, in agreement with the superior ORR activity revealed in the electrochemical studies.

To further evaluate the performance of the ZAB with CNDA900, galvanostatic discharge-charge cycling tests were carried out at 2.5 mA cm^{-2} for 30 min of charging and followed by 5 mA cm^{-2} for 15 min of discharging in each cycle. The cycling performances presented in Figure 4c show a good rechargeability over a period of 216 h of the ZAB containing the CNDA900 based air-cathode. Initially this required a charge voltage of 2.47 V and delivered a discharge voltage of 1.12 V, corresponding to a voltage gap of 1.35 V, comparable to the 1.33 V voltage gap of the ZAB containing the benchmark Pt/C catalyst (Figure 4d). After 50 h (Figure S11a), the difference between the charge and discharge cycles of CNDA900 decreased by 0.06 V to 1.29 V, resulting from a charge voltage of 2.43 V and a discharge voltage of 1.14 V. In comparison, the voltage gap of the Pt/C-based ZAB greatly increased to 1.45 V, 0.16 V higher than that of CNDA900. At this stage, the battery was already struggling to perform the charging process which greatly decreases the energy efficiency. After 181 h (Figure S11b), the Pt/C-based ZAB was unable to continue cycling whereas the one with CNDA900 continued charging at 2.5 V and discharging at 1.04 V maintaining a low voltage gap of 1.46 V. The CNDA900 based ZABs continuously cycled for 298 cycles confirming its rechargeability properties (Figure 4e). At this point, the battery required 2.36 V for the charging and delivered 1.04 V from the discharging process, leading to a reduced voltage gap of 1.32 V obtained by an increase of 0.1 mV per cycle over 216 h. The total discharge voltage presented a mere drop of 0.15 V (from 1.12 to 1.04 V; 0.27 mV per cycle) whereas the charge voltage decreased about 0.11 V (from 2.47 to 2.36 V; 0.37 mV per cycle). These results highlight the favourable catalytic activity of CNDA900 in ZABs originated from the high electron transport and electrocatalytic active sites distribution.

Conclusion

In summary, we have developed a facile strategy to introduce high N content onto a carbon framework without the use of templates, catalysts or harsh chemicals. We concluded that the interaction of the two π-conjugated polymers allowed the rearrangement of the carbon framework and distribution of extra N features from species originated from the decomposition of C_3N_4 during high temperature pyrolysis. Without the presence of PDA, C_3N_4 completely decomposed at temperatures above 750˚C. The activation and exposure of active sites within the matrix then resulted in an efficient ORR electrocatalyst. The results revealed that CNDA900 has a comparable $E_{1/2}$ and a remarkably improved diffusion-limited current density compared with other reported N-doped carbon catalysts. The composite catalyst also presented promising results towards the OER. The battery test data of ZABs containing CNDA900 confirmed their stability and practicality for a scalable production. The successful developments highlighted in this work provide an avenue for the fabrication of nitrogen-rich carbon-based catalysts for cost-effective and environmentally friendly ZABs.

Experimental Section

Materials and methods

Materials. Melamine (99%, Sigma-Aldrich), Trizma base [tris(hydroxymethyl)aminomethane, ≥ 99.9%, Sigma-Aldrich], dopamine hydrochloride (Sigma-Aldrich), potassium hydroxide (KOH, Merck KGaA), Nafion (5 wt% in alcohol and water, Sigma-Aldrich) and 20% platinum on carbon (Alfa Aesar) were directly used as received.

Synthesis of carbon nitride (C_3N_4). C_3N_4 was obtained by thermal polymerization of melamine. Typically, melamine (10 g) was placed in a porcelain crucible and heated to 550 °C at a ramping rate of 5 °C/min and kept at 550 °C for 4 h under Ar atmosphere. The sample was naturally cooled to room temperature and C_3N_4 was obtained with a yield of approximately 50%.

Synthesis of carbon nitride and dopamine-derived electrocatalysts (CNDA). CNDA was synthesized by polymerization of dopamine at the presence of C_3N_4 followed by carbonization. The polydopamine was prepared according to a previously reported study.[31] Typically, 500 mg of the as-prepared C_3N_4 was dispersed in 500 mL of 10 mM Tris-buffer solution (pH = 8.5) and the mixture was left to stir for 30 min. Subsequently, 500 mg of dopamine hydrochloride was added to the mixture and left to stir for another 20 h. The product was collected by centrifugation, repeatedly washed with deionized water and dried in an oven at 70 °C overnight. The dried sample was carbonized in a furnace at varied temperatures of 850, 900 and 950 °C, respectively, heated at a ramping rate of 5 °C/min and held at temperature for 1 h under Ar atmosphere. The final product was denoted CNDA850, CNDA900 and CNDA950, respectively. CNDA900 refers to the N-rich carbon hybrid catalyst synthesized at 900 °C, for instance. For comparison, carbonized-PDA (CPDA) was synthesised following the same procedure described above but without the C_3N_4 addition.

Material characterization. The morphologies and elemental mappings of the products were obtained by Field Emission-Scanning Electron Microscope (FE-SEM, JSM-7600F), Transmission Electron Microscope (TEM, Philips CM300) and Energy Dispersive X-Ray (EDX equipped on the SEM, Oxford INCA). The chemical compositions were investigated by X-ray Photoelectron Spectroscopy (XPS) using a Theta Probe electron spectrometer (VG ESCALAB200i-XL, Thermo Scientific). The binding energies were calibrated using C 1s peak at 284.4 eV. The crystallinity and phase composition of the samples were studied by X-ray Diffraction (XRD, Bruker D8 Discover GADDS with a Cu K_α radiation) and Raman spectroscopy (WITec alpha300-R, 532 nm laser excitation).

Electrochemical measurements. The electrocatalytic activity of the synthesised catalysts was investigated by Cyclic Voltammetry (CV) and Linear Sweep Voltammetry (LSV) measurements acquired from a Metrohm Autolab potentiostat/galvanostat (PGSTAT302N) station using a three-electrode system consisting of a Ag/AgCl (in saturated KCl) reference electrode, a Pt foil counter electrode and a glassy carbon working electrode (GC, 5 mm diameter). 0.1 M KOH solution saturated with O_2 or N_2 was used as the electrolyte. The working electrode was prepared by adding 10 mg of catalyst to a solution containing 2.2 mL of deionised water and 0.5 mL of Nafion (5 wt% in alcohol and water) and sonicating it for 30 mins to obtain a homogenous ink. An aliquot (8.3 µL) of this ink was drop-cast onto the GC electrode surface to obtain a theoretical catalyst loading of 0.2 mg cm^{-2}, unless otherwise stated. Pt/C and Ir/C electrodes were also prepared following the same procedure. From the LSV results, the number of electrons (n) transferred per O_2 molecule in ORR was calculated from the Koutecky-Levich (K-L) equation as follows:[53]

$$\frac{1}{J} = \frac{1}{J_L} + \frac{1}{J_K} = \frac{1}{B\omega^{1/2}} + \frac{1}{J_K} \quad (1)$$

$$B = 0.2nFC_0(D_0)^{2/3}\nu^{-1/6} \quad (2)$$

$$J_K = nFkC_0 \quad (3)$$

Where J is the measured current density, J_K and J_L are the kinetic limiting and diffusion limiting current densities, respectively, B is the Levich constant (determined by the inverse value of the slope of a straight linear fitting of the measured current densities, ω is the angular velocity of the electrode, F is the Faraday constant (96485 C mol^{-1}), C_0 is the concentration of dissolved O_2 in electrolyte solution (1.2×10^{-6} mol cm^{-3}), D_0 is the O_2 diffusion coefficient in KOH solution (1.9×10^{-5} cm^2 s^{-1}) and v is the kinetic viscosity of the electrolyte solution (0.01 cm^2 s^{-1}).[11,53] Both CV and LSV measurements were recorded with reference to the Ag/AgCl electrode. The potentials recorded by Ag/AgCl reference electrode potentials were calibrated with respect to the RHE potential according to the Nernst equation:

$$E_{RHE} = E_{Ag/AgCl} + 0.059pH + E^o_{Ag/AgCl} \quad (4)$$

Where E_{RHE} is the potential converted, $E_{Ag/AgCl}$ is the experimentally measured potential against the Ag/AgCl reference, the measured pH was 13 and $E^o_{Ag/AgCl} = 0.1976$ at 25 ˚C.[54,55]

Assembly and testing of Zn-air batteries (ZABs). The Zn-air cells were assembled using a polished zinc plate as the anode, an air cathode containing the CNDA900 or Pt/C catalyst and a 6 M KOH aqueous solution containing 0.1 M $ZnCl_2$ as the electrolyte. For the preparation of the cathode ink, a solution containing 50 mg of active catalyst and 10 mL of an aqueous Nafion solution (1 wt.%) was sonicated for 30 min. Then, this solution with calculated amount was drop-casted onto a carbon paper (Sigracet 38BC) to obtain a catalyst loading of 0.5 mg cm^{-2}. The electrode was then dried overnight at room temperature. The discharge and discharge-charge performances of ZABs were evaluated by the galvanostatic method on a battery tester (NEWARE BTS-610).

Acknowledgements

This research was supported by the University College London (UCL) and Agency for Science, Technology and Research (A*STAR), Singapore Research Attachment Programme (ARAP). The authors thank Mr Matej Sebek (UCL/IMRE) for his help with Raman characterization, Dr. Lim Poh Chong (IMRE) for his help with XRD data collection, Dr. Chai Jianwei (IMRE) for his help with XPS data collection and Dr Lin Ming and Ms. Siew Lang Teo (IMRE) for their help with TEM characterization.

Keywords: oxygen reduction reaction • nitrogen-rich carbon • carbon nitride • polydopamine • metal-air battery

References

[1] Y. Li, J. Lu, *ACS Energy Lett.* **2017**, *2*, 1370–1377.
[2] P. Gu, M. Zheng, Q. Zhao, X. Xiao, H. Xue, H. Pang, *J. Mater. Chem. A* **2017**, *5*, 7651–7666.
[3] J. Zhang, Z. Zhao, Z. Xia, L. Dai, *Nat. Nanotechnol.* **2015**, *10*, 444–452.
[4] X. Fu, X. Hu, Z. Yan, K. Lei, F. Li, F. Cheng, J. Chen, *Chem. Commun.* **2016**, *52*, 1725–1728.
[5] D. Guo, R. Shibuya, C. Akiba, S. Saji, T. Kondo, J. Nakamura, *Science (80-.).* **2016**, *351*, 361–365.
[6] J. S. Lee, S. T. Kim, R. Cao, N. S. Choi, M. Liu, K. T. Lee, J. Cho, *Adv. Energy Mater.* **2011**, *1*, 34–50.
[7] X. Zheng, X. Han, Y. Cao, Y. Zhang, D. Nordlund, J. Wang, S. Chou, H. Liu, L. Li, C. Zhong, Y. Deng, W. Hu, *Adv. Mater.* **2020**, *32*, 2000607.
[8] J. Song, S. Qiu, F. Hu, Y. Ding, S. Han, L. Li, H. Y. Chen, X. Han, C. Sun, S. Peng, *Adv. Funct. Mater.* **2021**, *31*, 2100618.
[9] D. Yu, Y. Ma, F. Hu, C. C. Lin, L. Li, H. Y. Chen, X. Han, S. Peng, *Adv. Energy Mater.* **2021**, *11*, 2101242.
[10] X. Han, X. Ling, Y. Wang, T. Ma, C. Zhong, W. Hu, Y. Deng, *Angew. Chemie - Int. Ed.* **2019**, *58*, 5359–5364.
[11] J. Shin, J. Guo, T. Zhao, Z. Guo, *Small* **2019**, *15*, DOI 10.1002/smll.201900296.
[12] T. Y. Ma, J. Ran, S. Dai, M. Jaroniec, S. Z. Qiao, *Angew. Chemie - Int. Ed.* **2015**, *54*, 4646–4650.
[13] I. M. Patil, M. Lokanathan, B. Kakade, *J. Mater. Chem. A* **2016**, *4*, 4506–4515.
[14] J. Li, Y. Zhang, X. Zhang, J. Han, Y. Wang, L. Gu, Z. Zhang, X. Wang, J. Jian, P. Xu, B. Song, *ACS Appl. Mater. Interfaces* **2015**, *7*, 19626–19634.
[15] K. Qu, Y. Zheng, S. Dai, S. Z. Qiao, *Nano Energy* **2016**, *19*, 373–381.
[16] Y. Zheng, Y. Jiao, L. Ge, M. Jaroniec, S. Z. Qiao, *Angew. Chemie* **2013**, *125*, 3192–3198.
[17] Y. P. Zhu, Y. Liu, Y. P. Liu, T. Z. Ren, G. H. Du, T. Chen, Z. Y. Yuan, *J. Mater. Chem. A* **2015**, *3*, 11725–11729.
[18] J. Liang, X. Du, C. Gibson, X. W. Du, S. Z. Qiao, *Adv. Mater.* **2013**, *25*, 6226–6231.
[19] L. Hadidi, E. Davari, M. Iqbal, T. K. Purkait, D. G. Ivey, J. G. C. Veinot, *Nanoscale* **2015**, *7*, 20547–20556.
[20] V. V. Strelko, V. S. Kuts, P. A. Thrower, *Carbon N. Y.* **2000**, *38*, 1499–1503.
[21] M. Qiao, C. Tang, G. He, K. Qiu, R. Binions, I. P. Parkin, Q. Zhang, Z. Guo, M. M. Titirici, *J. Mater. Chem. A* **2016**, *4*, 12658–12666.
[22] M. Seredych, K. László, E. Rodríguez-Castellón, T. J. Bandosz, *J. Energy Chem.* **2016**, *25*, 236–245.
[23] N. Daems, X. Sheng, I. F. J. Vankelecom, P. P. Pescarmona, *J. Mater. Chem. A* **2014**, *2*, 4085–4110.
[24] H. Yu, L. Shang, T. Bian, R. Shi, G. I. N. Waterhouse, Y. Zhao, C. Zhou, L. Z. Wu, C. H. Tung, T. Zhang, *Adv. Mater.* **2016**, *28*, 5080–5086.
[25] K. Qiu, G. Chai, C. Jiang, M. Ling, J. Tang, Z. Guo, *ACS Catal.* **2016**, *6*, 3558–3568.
[26] W. Wei, H. Liang, K. Parvez, X. Zhuang, X. Feng, K. Müllen, *Angew. Chemie - Int. Ed.* **2014**, *53*, 1570–1574.
[27] W. He, C. Jiang, J. Wang, L. Lu, *Angew. Chemie - Int. Ed.* **2014**, *53*, 9503–9507.
[28] S. Chen, J. Duan, M. Jaroniec, S. Z. Qiao, *Adv. Mater.* **2014**, *26*, 2925–2930.
[29] J. Zhang, Y. Sun, J. Zhu, Z. Gao, S. Li, S. Mu, Y. Huang, *Adv. Sci.* **2018**, *5*, 1–7.
[30] J. Xu, F. Xu, M. Qian, F. Xu, Z. Hong, F. Huang, *Adv. Mater.* **2017**, *29*, 1–8.
[31] B. Li, Y. Chen, X. Ge, J. Chai, X. Zhang, T. S. A. Hor, G. Du, Z. Liu, H. Zhang, Y. Zong, *Nanoscale* **2016**, *8*, 5067–5075.
[32] K. Qu, Y. Wang, X. Zhang, H. Chen, H. Li, B. Chen, H. Zhou, D. Li, Y. Zheng, S. Dai, *ChemNanoMat* **2018**, *4*, 417–422.
[33] K. Qu, Y. Wang, A. Vasileff, Y. Jiao, H. Chen, Y. Zheng, *J. Mater. Chem. A* **2018**, *6*, 21827–21846.
[34] Y. Tang, J. Chen, X. Wang, X. Wang, Y. Zhao, Z. Mao, D. Wang, *Electrochim. Acta* **2019**, *324*, 134880.
[35] Z. Liang, H. Zheng, R. Cao, *ChemElectroChem* **2019**, *6*, 2600–2614.
[36] D. N. Nguyen, U. Sim, J. K. Kim, *Polymers (Basel).* **2020**, *12*, 912.
[37] Q. Shi, Y. Ma, L. Qin, B. Tang, W. Yang, Q. Liu, *ChemElectroChem* **2019**, *6*, 2924–2930.
[38] Y. P. Zhu, C. Guo, Y. Zheng, S. Z. Qiao, *Acc. Chem. Res.* **2017**, *50*, 915–923.
[39] Z. Lin, G. H. Waller, Y. Liu, M. Liu, C. P. Wong, *Carbon N. Y.* **2013**, *53*, 130–136.
[40] X. Liu, J. Kang, Y. Dai, C. Dong, X. Guo, X. Jia, *Adv. Mater. Interfaces* **2018**, *5*, DOI 10.1002/admi.201800303.
[41] W. Yang, L. Hou, X. Xu, Z. Li, X. Ma, F. Yang, Y. Li, *Carbon N. Y.* **2018**, *130*, 325–332.
[42] K. Ai, Y. Liu, C. Ruan, L. Lu, G. Lu, *Adv. Mater.* **2013**, *25*, 998–1003.
[43] R. Li, K. Parvez, F. Hinkel, X. Feng, K. Müllen, *Angew. Chemie - Int. Ed.* **2013**, *52*, 5535–5538.
[44] Z. Yu, F. Li, Q. Yang, H. Shi, Q. Chen, M. Xu, *ACS Sustain. Chem. Eng.* **2017**, *5*, 7840–7850.
[45] M. R. Gholipour, F. Béland, T. O. Do, *ACS Sustain. Chem. Eng.* **2017**, *5*, 213–220.
[46] W. J. Ong, L. L. Tan, S. P. Chai, S. T. Yong, A. R. Mohamed, *Nano Energy* **2015**, *13*, 757–770.
[47] K. Zhong, Y. Wang, Q. Wu, H. You, H. Zhang, M. Su, R. Liang, J. Zuo, S. Yang, J. Tang, *J. Power Sources* **2020**, *467*, 228313.
[48] H. Luo, C. Gu, W. Zheng, F. Dai, X. Wang, Z. Zheng, *RSC Adv.* **2015**, *5*, 13470–13477.
[49] S. S. Shinde, C. H. Lee, A. Sami, D. H. Kim, S. U. Lee, J. H. Lee, *ACS Nano* **2017**, *11*, 347–357.
[50] P. Zhang, D. Bin, J. S. Wei, X. Q. Niu, X. B. Chen, Y. Y. Xia, H. M. Xiong, *ACS Appl. Mater. Interfaces* **2019**, *11*, 14085–14094.
[51] Z. Guo, F. Wang, Y. Xia, J. Li, A. G. Tamirat, Y. Liu, L. Wang, Y. Wang, Y. Xia, *J. Mater. Chem. A* **2018**, *6*, 1443–1453.
[52] Y. Liang, Y. Li, H. Wang, J. Zhou, J. Wang, T. Regier, H. Dai, *Nat. Mater.* **2011**, *10*, 780–786.
[53] A. J. Bard, L. R. Faulkner, *Electrochemical Methods: Fundamentals and Applications*, **2001**.
[54] S. Hoang, S. Guo, N. T. Hahn, A. J. Bard, C. B. Mullins, *Nano Lett.* **2012**, *12*, 26–32.
[55] M. Nunes, I. M. Rocha, D. M. Fernandes, A. S. Mestre, C. N. Moura, A. P. Carvalho, M. F. R. Pereira, C. Freire, *RSC Adv.* **2015**, *5*, 102919–102931.

10.1002/celc.202100865

Entry for the Table of Contents

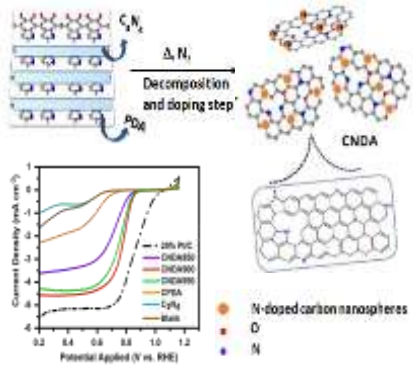

A facile strategy to produce an efficient and durable ORR electrocatalyst based on the incorporation of two benign and scalable precursors, polydopamine (PDA) and C_3N_4 (carbon nitride), without the use of catalysts or harsh chemicals, was developed. This combination allowed the doping of extra nitrogen features from species originated from the decomposition of C_3N_4. Further rearrangement of the carbon framework and high N content (12.5 at.%) resulted in the activation and exposure of active sites within the matrix.